nature geoscience

SUPPLEMENTARY INFORMATION

DOI: 10.1038/NGEO629

# Supplementary Online Materials for 'Sinking Deltas'

*James P.M. Syvitski[1], Albert J. Kettner[1], Irina Overeem[1], Eric W.H. Hutton[1], Mark T. Hannon[1], G. Robert Brakenridge[2], John Day[3], Charles Vörösmarty[4], Yoshiki Saito[5], Liviu Giosan[6], Robert J. Nicholls[7]*

[1]CSDMS Integration Facility, INSTAAR, U. Colorado, Boulder CO, 80309-0545
[2]Dartmouth Flood Observatory, Dartmouth College, Hanover, NH 03755
[3]Dept. of Oceanography and Coastal Sciences, Louisiana State U., Baton Rouge, LA 70803
[4]Dept. Civil Engineering, City College of New York, City University of New York, NY 10035
[5]Geological Survey of Japan, AIST, Tsukuba 305-8567, Japan
[6]Woods Hole Oceanographic Institution, Woods Hole, MA 02543
[7]School of Civil Engineering and the Environment and Tyndall Centre for Climate Change Research, University of Southampton, SO17 IBJ UK

## Shuttle Radar Topography Mission (SRTM)

The NASA, NGA (formerly NIMA) Shuttle Radar Topography Mission (SRTM) obtained interferometric synthetic aperture radar (InSAR) data during an 11-day mission to generate high-resolution digital elevation data for ≈80% of the Earth landmass, located between 60°N and 59°S (Farr et al., 2007). The vertical precision of SRTM data depends considerably on location, terrain characteristics and surface feature properties. We employ the SRTM C-band data with a 5.6 cm wavelength, with its near global relative vertical accuracy of ≈ 3.7 m (Berry et al., 2007), and for many of the world's flat-lying (deltaic) areas a vertical RMSE (root mean square error) between 1.1 to 1.6 m (Schumann et al. 2008). The horizontal footprint of a SRTM pixel is either 1-arc or 3-arc seconds, depending on data availability. The C band monitored 99.96% of the targeted landmass at least once, 94.59% at least twice, and ~50% three or more times (Farr et al., 2007).

Since ocean heights tidally-varied over the duration of the mission, the SRTM DEM consisted of the static heights over land and tidally adjusted TOPEX/Poseidon–derived ocean heights (Farr et al., 2007). A vector shoreline database (the SRTM Water Body Data Set) produced by NGA depicted the ocean coastlines, lake shorelines, and rivers. The ocean elevation was set to 0 m, lakes of 600 m or more in length were flattened to a constant height, and rivers that exceeded 183 m in width were delineated and monotonically stepped down in height (Farr et al., 2007).

Thirty-three representative deltas were examined using SRTM altimetry, binned at 1 m intervals (Table 1, Figs. 1-3 of main paper]. The deltas were examined for the extent and location of areas near or below sea level, and for geomorphic patterns that would provide insight into a delta's morphodynamics (e.g. number of distributary channels, abandoned channels, crevasse splays and other river flood deposits, tidal channels, beach ridges, lagoons, e.g. see Syvitski and Saito, 2007, Woodroffe et al., 2006. Land-use on most deltas is agricultural. Deltas with a substantive canopy (e.g. Niger, Orinoco, Amazon) would under-predict areas registering near, at or below sea level (Table 1), although the C radar penetrates significantly into a vegetation canopy (Farr et al., 2007). The Amur Delta has the potential for snowdrifts errors (SRTM was conducted in February), though the C radar would likely penetrate into the drifts (Farr et al., 2007).

**Supplementary Figure 1: Location map of the representative deltas used in this study.**

## Flood Inundation

MODIS imagery comes from the Moderate Resolution Imaging Spectroradiometer onboard NASA's Aqua and Terra satellites, part of the NASA-centered international Earth Observing System. Each satellite flies in a polar orbit, to daily image much of the earth. Terra provides morning images; Aqua provides images a few hours later (afternoon). MODIS near-infrared composites employ the following wavelengths: 2,155 nm, 876 nm, 670 nm, wherein vegetation appears green, bare soil appears pink, water appears black, and suspended sediments appear various shades of blue depending on their concentration.

DOI: 10.1038/NGEO629

MODIS true color imagery uses the 670 nm, 565 nm, and 479 nm wavelengths, which are sufficient to distinguish turbid water from water with low sediment concentrations.

MODIS imagery at a maximum horizontal resolution of 250 m provides little ground surface information during periods of storms, due to cloud cover. However, hurricanes often are followed by cloud free days, making storm surge assessment possible, albeit with conservative estimates since the peak levels are often not recorded. For example imagery following Cyclone Nargis that impacted Myanmar was available within three days of landfall (Fig. 2). Similar useful imagery of river flooding, such as following intense periods of monsoonal rainfall, is often available within days and analyzed in detail, for example, at the Dartmouth Flood Observatory (DFO) (e.g. Fig. 2). Area inundated by storm surges, river floods, or in situ flooding, all since 1998, is based on MODIS imagery or DFO maps (Table 1; Supplementary Figure 2).

**Supplementary Figure 2:** Portions of flood maps of representative deltas and their floodplains produced by the Dartmouth Flood Observatory (see text) which show the extent of floodwaters over the last decade, shown with various shades in blue that represent different years). A) Mahanadi and Brahmani deltas, India; B) Chao Phraya delta, Thailand; C) Danube, Romania; D) Krishna and Godavari deltas, India; and E) and F) Ganges-Brahmaputra delta complex, Bangladesh and India; G); Indus, Pakistan; H) Mekong, Vietnam; I) Po, Italy; J) Pearl, China; K) Rhone, France; L) Magdalena, Columbia; M) Mississippi, USA; N) Niger, Nigeria; O) Limpopo, Mozambique; P) Parana, Argentina; Q) Old and new Yellow River delta and Yangtze deltas, China; R) Tigris-Euphrates, Iraq; S) Orinoco, Venezuela.

## Example imagery of type floods

**Supplementary Figure 3:** MODIS (Visible) images of the Krishna (lower left) and Godavari (mid) deltas, east coast of India. Receiving similar rain, the reservoir trapping of the Krishna is more effective, resulting in little transport of sediment to the delta. The Godavari has less reservoir trapping and more sediment enters its coast. Flood controls pass most of this turbid water through the delta, with little sediment retention on the delta.

**Supplementary Figure 4:** Changes in flooded areas on the Krishna and Godavari deltas, as seen from near infrared MODIS images.

**Supplementary Figure 5:** Remarkable set of visible wavelength MODIS satellite imagery of the Mahanadi and Brahmani deltas, India. The lower (Mahanadi) delta has much of its sediment trapped in reservoirs and little sediment enters or exits the delta. The upper (Brahmani) delta sees more turbid floodwaters able to deposit sediment on the delta.

**Supplementary Figure 6:** Sequence of MODIS near-IR images of the Mahanadi and Brahmani deltas on the East coast of India. The sequence shows the flooding of the deltas, and the eventual drying.

**Supplementary Figure 7:** MODIS (visible) images of a December flood of the Mississippi, showing the pathway of the turbid plumes emanating from delta distributary channels.

**Supplementary Figure 8:** April 15, 2008, MODIS (Aqua) 19:13 UTC, Mississippi under Flood.

## Historical Maps

Historical maps (published between 1674 and 1922) of the major world deltas were georectified using the location of historical towns and cities, and unique land features (e.g. Fig. 4). Older cartographic surveys often did not have the appropriate resolution for this study. Distributary channels from the historical maps with a mean location error of less than 6 km were digitized and combined with satellite imagery to aid in interpretation of older and abandoned distributary channels observed in the satellite imagery. Of the approximately >200 maps obtained, 86 had the requisite resolution as indicated in Table 1 (Supplementary Fig. 10). Distributary channel reduction (Table 1) is from historical map analysis compared to modern imagery (for details see Syvitski and Saito, 2007).

**Supplementary Figure 9:** Representative historical maps. A) Danube 1922; B) Mahanadi and Brahmani 1872; C) Chao Phraya 1844; D) Amazon 1844; E) Ganges 1794; F) Gadaveri 1832; G) Indus 1829; H) Indus 1922; I) Krishna 1832; J) Irawaddy 1844; K) Magdalena 1820; L) Mekong 1922; M) Mississippi 1895; N) Niger Delta 1832; O) Nile 1802; P) Orinoco 1840; Q) Parana 1873; R) Pearl 1843; S) Po 1645; T) Rhone 1814; U) Tigris-Euphrates 1831; V) Vistula 1787; W) Yangtze & Old Yellow 1747.

## Subsidence and Relative Sea Level Rates

Relative Sea level Rise values (Table 1) are based on subsidence rates from literature sources (e.g. Saito et al., 2007; Rodolpho et al., 2006) and from the Permanent Service for Mean Sea Level (PSMSL), hosted at the Proudman Oceanographic Laboratory (POL). The Permanent Service for Mean Sea Level (PSMSL) was established in 1933, and is the global data bank for long-term sea level change information from several hundred tide gauges situated all over the globe." A data catalogue is available from http://www.pol.ac.uk/psmsl/pub/catalog.dat. Supplementary Table 1 provides the details of the station locations, and detailed data files for each station. Stations outside of the delta areas were not used in our analysis but provide an indication of regional sea level changes. A word of caution on *Subsidence* or *Relative Sea Level Rise* rates: often rates in the literature are maximum rates within a deltaic area — the rates are not area-integrated; whereas *Aggradation* rates refer to area-integrated rates. Subsurface mining activity is from a literature survey (e.g. Syvitski, 2008; Ericson et al., 2005).

**Supplementary Table 1:** PSMSL tide trend data of representative deltas

| Delta | # of stations | Start yr | End yr | data cover | Tot. # yrs | Delta change mm/yr | Off-delta change mm/yr | Trend R2 | Comments |
|---|---|---|---|---|---|---|---|---|---|
| Amazon, Brazil | 2 | 1952 | 1955 | 4 | 4 | | | 0.11 | SE close to delta |
| Amur, Russia | | | | | | | | | NO DATA |
| Brahmani, India | 1 | 1967 | 2005 | 21 | 39 | 1.33 | | 0.09 | ON DELTA |
| Chao Phraya, Thai. | 2 | 1940 | 2006 | 63 | 67 | 13.19 | | 0.80 | On Delta |
| Colorado, Mexico | 1 | 1973 | 1989 | 10 | 17 | | 5.05 | 0.57 | Far S of Delta |
| Congo, DRC | 1 | 1977 | 1979 | 3 | 3 | | | 0.49 | Far N of delta |
| Danube, Romania | 1 | 1933 | 1996 | 59 | 64 | | 1.19 | 0.09 | S of Delta |
| Fly, PNG | 1 | 1958 | 1959 | 2 | 2 | | | 1.00 | Far E of delta |
| Ganges, Bangl. | 10 | 1932 | 2005 | 66 | 74 | 8.35 | | 0.74 | On Delta |
| Godavari, India | 2 | 1937 | 2005 | 54 | 69 | | 0.76 | 0.13 | NNE of Delta |
| Han, Korea | 1 | 1960 | 2006 | 39 | 47 | | 0.62 | 0.04 | SE of Delta |
| Indus, Pakistan | 1 | 1916 | 1992 | 44 | 77 | | 0.61 | 0.08 | Off Delta |
| Irrawaddy, Myan. | 3 | 1916 | 1962 | 25 | 47 | 3.38 | | 0.35 | On Delta |
| Krishna, India | 2 | 1937 | 2005 | 54 | 69 | | 0.76 | 0.13 | NE of Delta |
| Limpopo, Moz. | 1 | 1961 | 2000 | 12 | 40 | | 0.31 | 0.05 | SW of Delta |
| Magdalena, Col. | 2 | 1949 | 1992 | 38 | 44 | 5.27 | | 0.93 | SW of Delta |
| Mahakam, Borneo | | | | | | | | | No Data |
| Mahanadi, India | 1 | 1967 | 2005 | 21 | 39 | 1.33 | | 0.09 | On Delta |
| Mekong, Vietnam | 1 | 1979 | 2001 | 22 | 23 | 5.75 | | 0.51 | E of Delta |
| Mississippi, USA | 2 | 1947 | 2006 | 56 | 60 | 9.27 | | 0.93 | On delta |
| Niger, Nigeria | 1 | 1969 | 1972 | 4 | 4 | 32.40 | | 0.65 | On Delta |
| Nile, Egypt | 1 | 1923 | 1946 | 24 | 24 | 4.80 | | 0.53 | On Delta |
| Orinoco, Venez. | 3 | 1955 | 1962 | 8 | 8 | | | 0.00 | Off delta |
| Parana, Argentina | 4 | 1905 | 1987 | 83 | 83 | 1.57 | | 0.39 | On delta |
| Pearl, China | 1 | 1925 | 1982 | 58 | 58 | 0.25 | | 0.01 | On delta |
| Po, Italy | 2 | 1909 | 2000 | 83 | 92 | | 2.40 | 0.74 | Far from Delta |
| Rhone, France | 1 | 1885 | 2006 | 115 | 122 | | 1.23 | 0.71 | E of Delta |
| Sao Francisco, Bra. | 1 | 1949 | 1968 | 19 | 20 | | 2.68 | 0.67 | S of Delta |
| Tigris, Iraq | 1 | 1979 | 2004 | 13 | 26 | | 3.59 | 0.69 | S of Delta |
| Tone, Japan | 2 | 1982 | 2007 | 26 | 26 | 2.28 | | 0.51 | On Delta |
| Vistula, Poland | 4 | 1926 | 1986 | 52 | 61 | | 1.77 | 0.24 | NE of Delta |
| Yangtze, China | 1 | 1969 | 2007 | 29 | 39 | 5.63 | | 0.83 | N of Delta |
| Yellow, China | | | | | | | | | No Data |
| Average | | | | | | 6.77 | 1.75 | | |

DOI: 10.1038/NGEO629

## Hurricane data

Hurricane Information was obtained from the online Unisys Weather Service dealing with hurricanes (cyclones, typhoons) http://weather.unisys.com/hurricane/index.html, providing hurricane information including the track of the storm and other tracking information (latitude and longitude, maximum sustained winds in knots, and central pressure in millibars). Value added information is also available at the NOAA National Weather Service, National Hurricane Center Archive http://www.nhc.noaa.gov/archive/. The Unisys data and plots coverage is as follows: 1) Atlantic: 1995-2008 (with Best Tracks from 1851-2007); 2) East Pacific: 1997-2008 (with Best Tracks from 1949-2005); 3) West Pacific: 1996-2008 (with Best Tracks from 1945-2003); 4) South Pacific: 2000-2008; 5) South Indian: 2000-2008 (with Best Tracks from 1949-2003); and 6) North Indian: 2000-2008 (with Best Tracks from 1945-2003). Further details from the Tropical Advisory Archive: http://weather.unisys.com/hurricane/archive/. Supplementary Figure 11 shows the Saffir-Simpson scale of hurricanes in terms of type, category, pressure, wind speed, typical surge height and track.

**Supplementary Figure 10:** Study deltas are located with red stars on this Unisys storm track map.

## *SOM References*

Berry, P.A.M., Garlick, J.D., Smith, R.G., 2007. Near-global validation of the SRTM DEM using satellite radar altimetry. Remote Sensing of Environment 106 (1), 17–27.

Coleman, J,M., Roberts, H.H., Stone, G.W., 1998. Mississippi driver Delta: an Overview. Journal of Coastal Research, 14 (3): 698-716.

Ericson, J.P., Vörösmarty, C.J., Dingman, S.L., Ward, L.G., Meybeck, M., 2006. Effective sea-level rise and deltas: causes of change and human dimension implications. Global and Planetary Change 50, 63-82.

Farr, T.G., Rosen, P.A., Caro, E., Crippen, R., Duren, R., Hensley, S., Kobrick, M., Paller, M., Rodriguez, E., Roth, L., Seal, D., Shaffer, S., Shimada, J., Umland, J., Werner, M., Oskin, M., Burbank, D., and Alsdorf, D., (2007) The Shuttle Radar Topography Mission. *Reviews of Geophysics*, 45, RG2004, doi:10.1029/2005RG000183.

Kesel, R., 1988. The decline in the suspended load of the Lower Mississippi River and its influence on adjacent wetlands. Environmental Geology 11, 3.DOI 10.1007/BF02574816.

Meade, R. H., and Parker, R.S. 1985, Sediment in rivers of the United States:in: National Water Survey 1984, U.S. Geological Survey Water-Supply Paper 2275, p. 49–60.

Milliman, J.D. and Syvitski, J.P.M. 1992. Geomorphic/tectonic control of sediment discharge to the ocean: The importance of small mountainous rivers. Journal of Geology 100: 525-544.

Roldolfo, K.S., and Siringan, F.P., 2006, Global sea-level rise is recognised, but flooding from anthropogenic land subsidence is ignored around northern Manila Bay, Philippines. Disasters, 30(1): 118–139.

Saito Y., Chaimanee N., Jarupongsakul, T., and Syvitski, J.P.M. 2007. Shrinking megadeltas in Asia: Sea-level rise and sediment reduction impacts from case study of the Chao Phraya delta. Inprint Newsletter of the IGBP/IHDP Land Ocean Interaction in the Coastal Zone 2007/2: 3-9.

Schumann, G., P. Matgen, M.E.J. Cutler, A. Black, L. Hoffmann, L. Pfister, 2008, Comparison of remotely sensed water stages from LiDAR, topographic contours and SRTM. ISPRS Journal of Photogrammetry & Remote Sensing 63: 283-296.

Syvitski, J.P.M., 2008, Deltas at Risk. Sustainability Science, 3: 23-32.

Syvitski, J.P.M. and Milliman, J.D., 2007, Geology, geography and humans battle for dominance over the delivery of sediment to the coastal ocean. J. Geology, 115: 1-19.

Syvitski, J.P.M., Kettner, A.J., Correggiari, A., Nelson, B.W. 2005, Distributary channels and their impact on sediment dispersal. Marine Geology 222-223: 75-94.

Syvitski, J.P.M., Saito, Y. 2007, Morphodynamics of Deltas under the Influence of Humans. Global and Planetary Changes 57: 261-282.

Woodroffe, C.D., Nicholls, R.J., Saito, Y., Chen, Z., and Goodbred, S.L., 2006. Landscape variability and the response of Asian megadeltas to environmental change. In Harvey, N., ed., Global Change and Integrated Coastal Management: the Asia-Pacific Region. Coastal Systems and Continental Margins, Vol. 10. Springer, pp. 277–314.

**Other Key References On Deltas And Subsidence**

Stephens, J.C., Allen, L.H., Chen, E. Organic soil subsidence. in *Man-Induced Land Subsidence,* T.L. Holzer Ed., Rev. Eng. Geol. Ser. **VI**, 107-122 (1984).

Morton, R.A., Bernier. J.C., Barras, J.A. & Ferina, N.F. *Rapid subsidence and historical wetland loss in the Mississippi delta plain: likely causes and future implications*. USGS Open File Report **2005-1216**, 124 pp. (2005).

Abam, T.K.S. Regional hydrological research perspective in the Niger Delta *Hydrological Sciences* **46**, 13-25 (2001).

Bondesan, M., Simeoni, U. Dinamica e analisi morfologica statistica dei litorali del delta del Po e alle foci dell'Adige e del Brenta. *Mem. Sci. Geol.* **36**, 1-48 (1983).

Simeoni, U., Fontolan, G., Tessari, U. & Corbau, C. Domains of spit evolution in the Goro area, Po Delta, Italy. *Geomorphology* **86**, 332-348 (2007).

Yu, L. The Huanghe (Yellow) River: Recent changes and its countermeasures. *Cont. Shelf Res.* **26**, 2281-2298 (2006).

J.W. Day, Jr., *et al*. Pattern and process of land loss in the Mississippi Delta: A Spatial and Temporal Analysis of Wetland habitat change. *Estuaries* **23**, 425-438 (2000).

Ericson, J.P., Vörösmarty, C.J., Dingman, S.L., Ward, L.G. & Meybeck, M. Effective sea-level rise and deltas: causes of change and human dimension implications. *Global Planet. Change* **50**, 63-82 (2006).

DOI: 10.1038/NGEO629

FIGURE 1

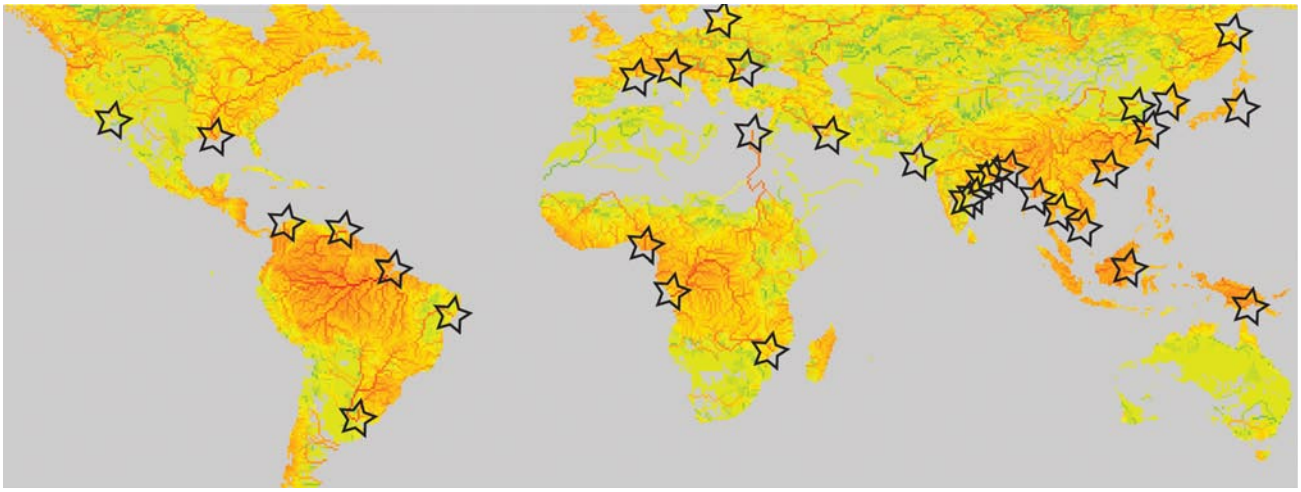

FIGURE 2

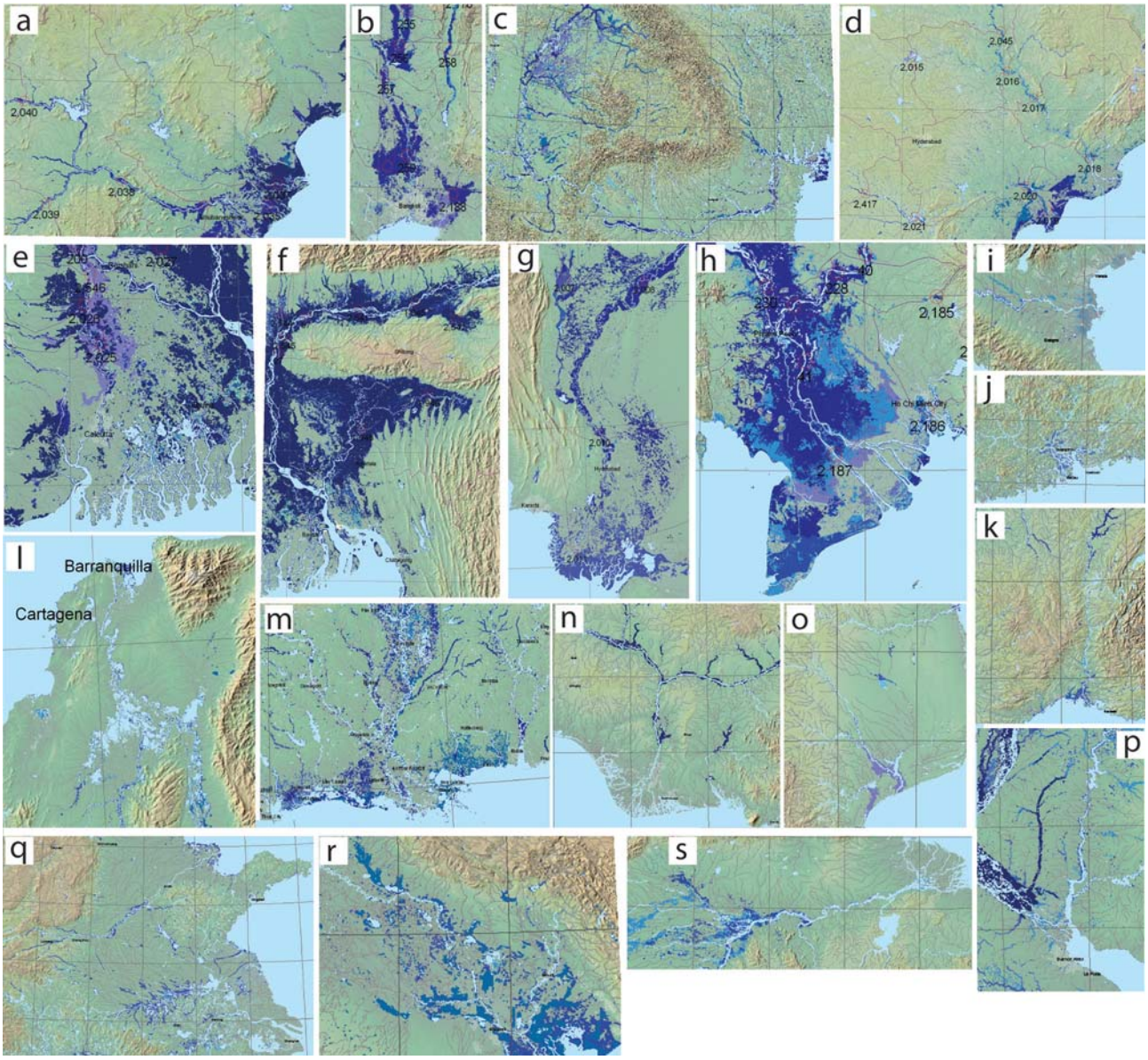

DOI: 10.1038/NGEO629

FIGURE 3

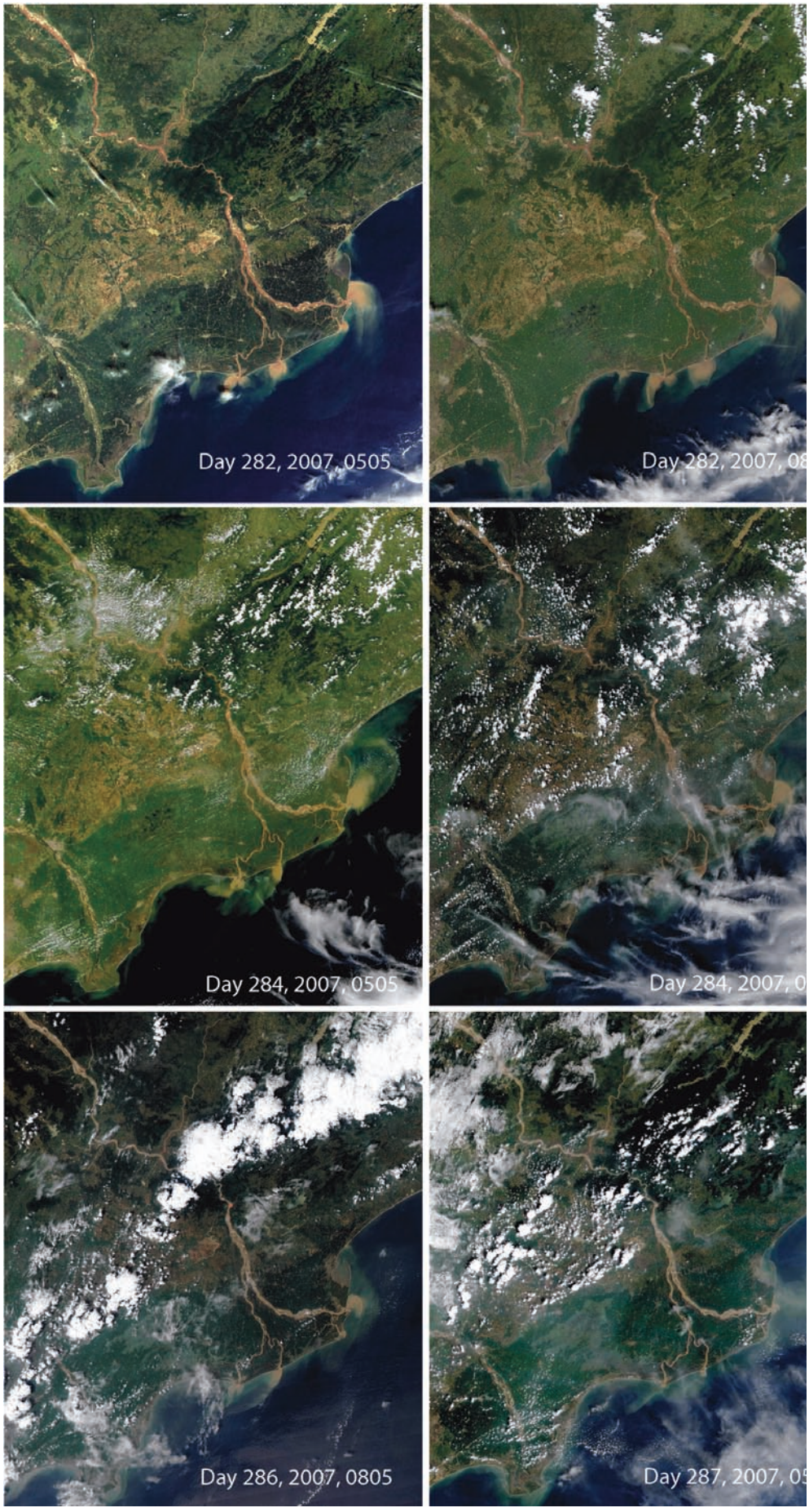

FIGURE 4

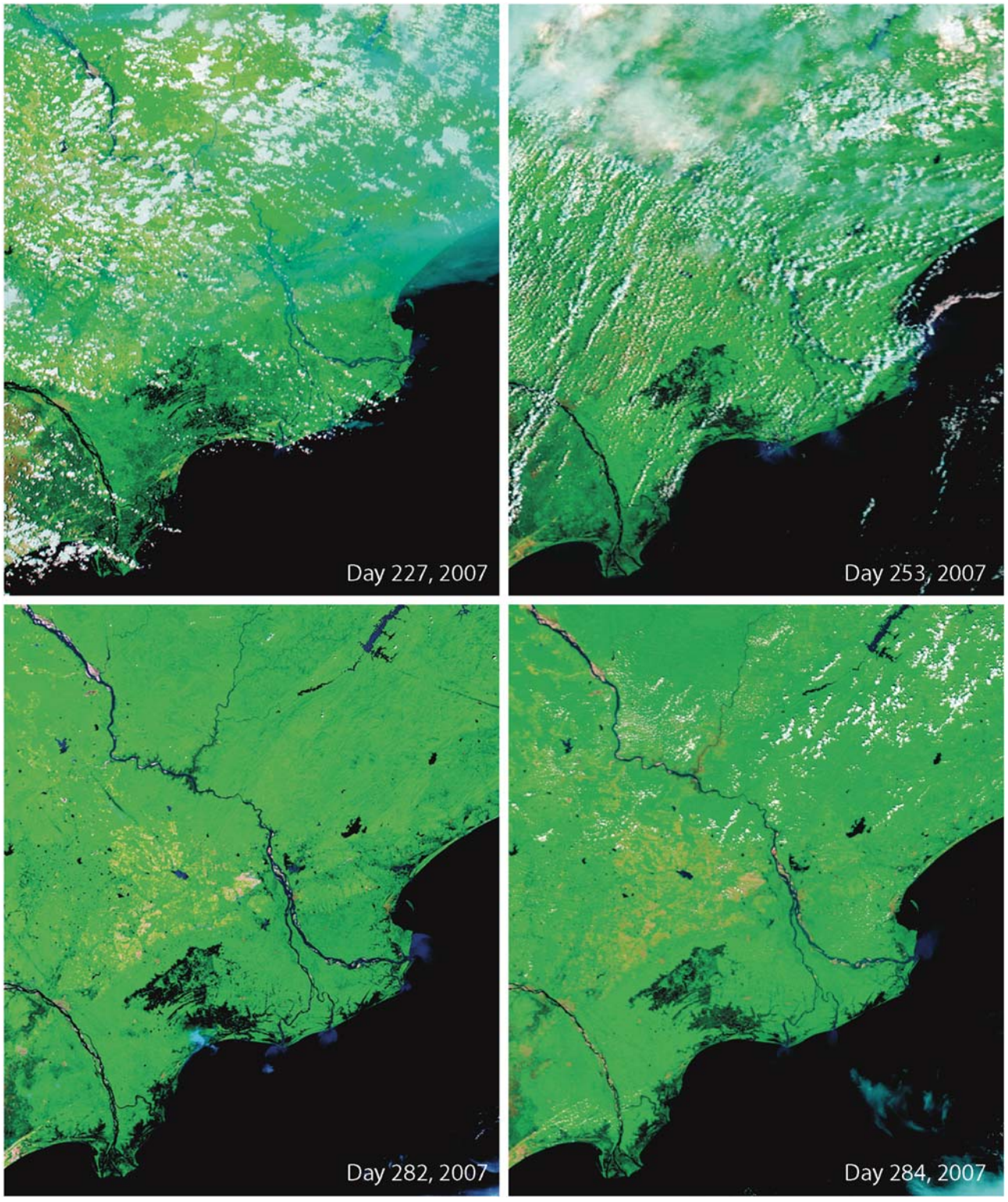

DOI: 10.1038/NGEO629

FIGURE 5

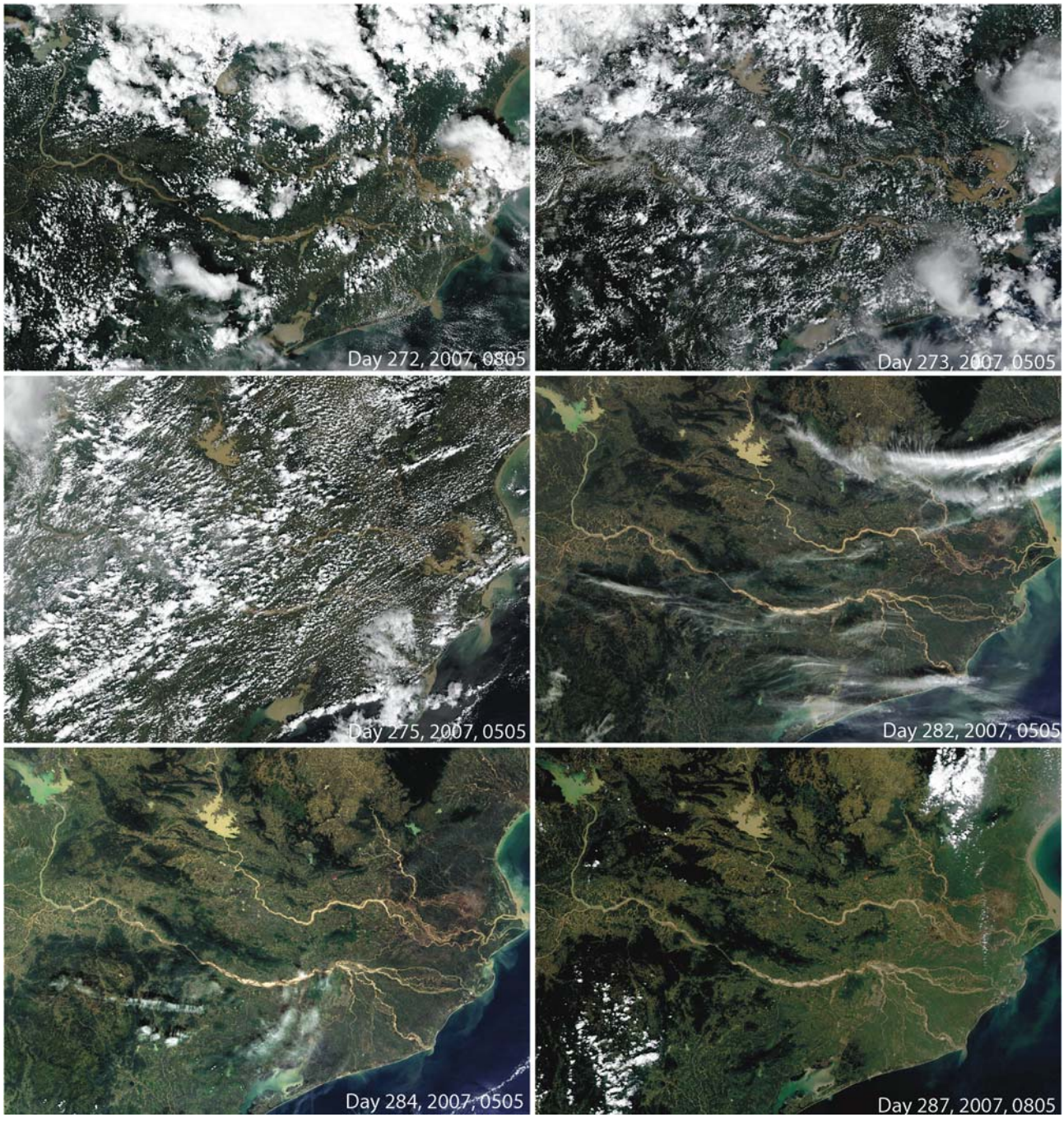

FIGURE 6

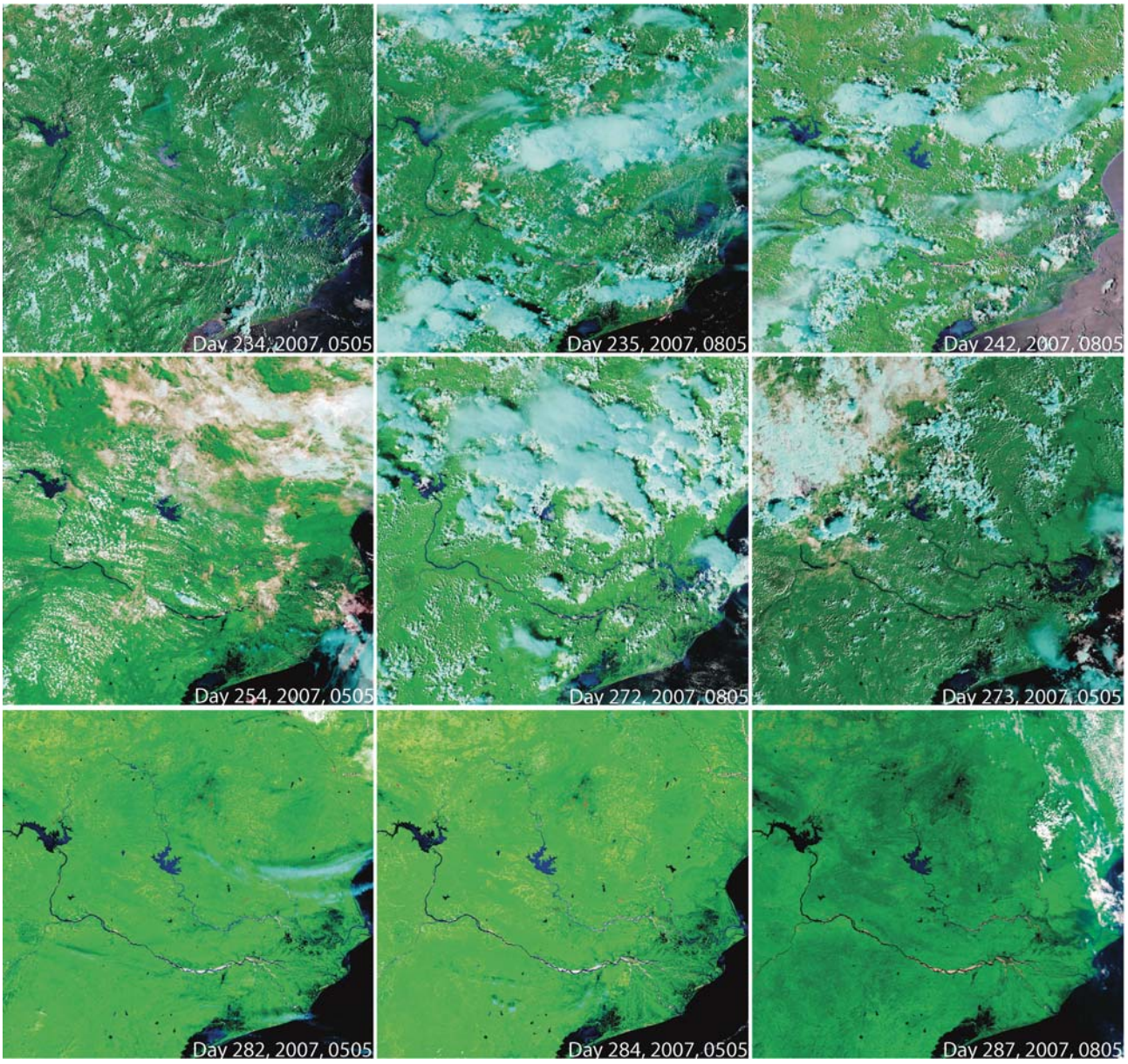
Day 234, 2007, 0505
Day 235, 2007, 0805
Day 242, 2007, 0805
Day 254, 2007, 0505
Day 272, 2007, 0805
Day 273, 2007, 0505
Day 282, 2007, 0505
Day 284, 2007, 0505
Day 287, 2007, 0805

DOI: 10.1038/NGEO629

FIGURE 7

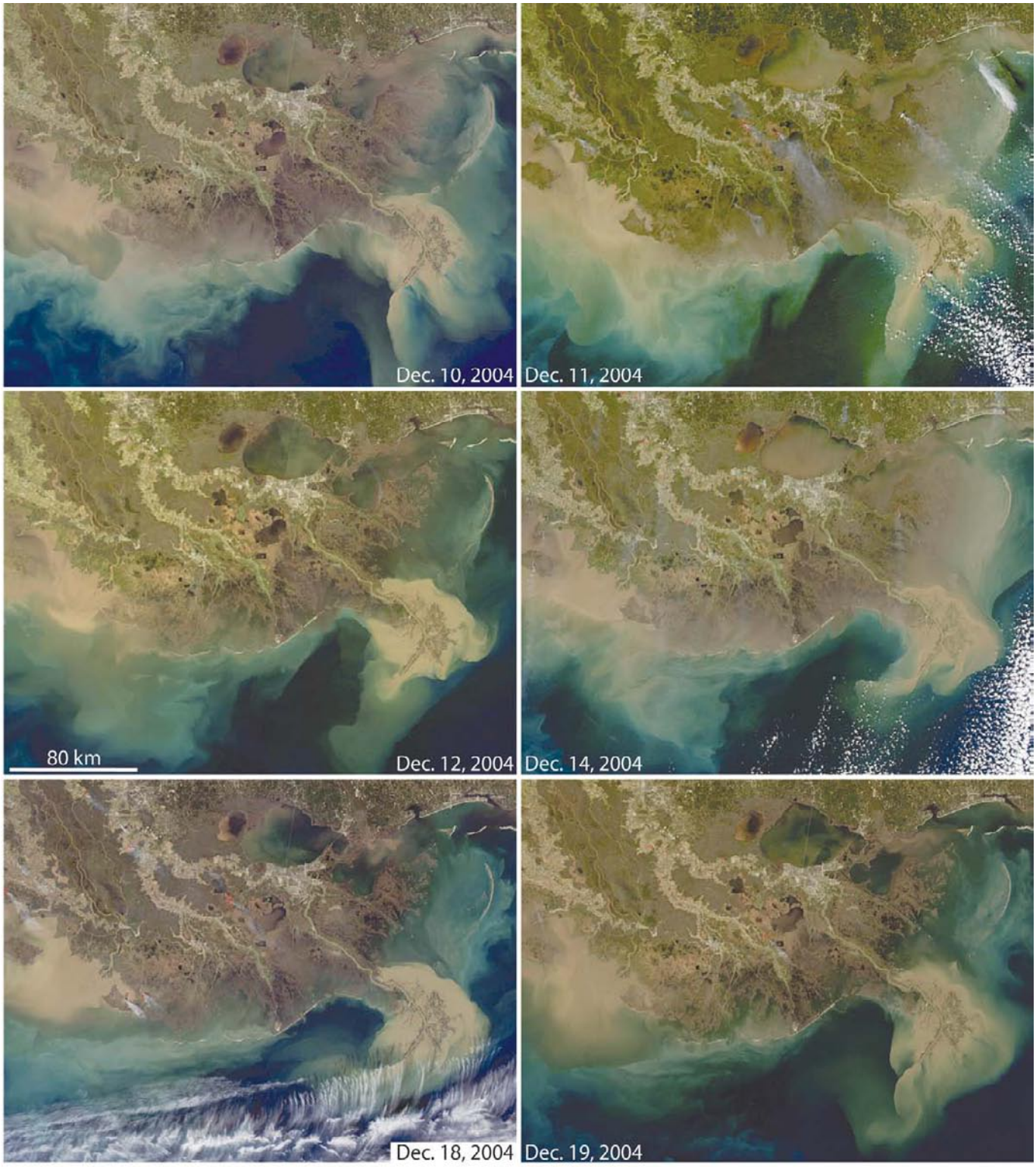

FIGURE 8

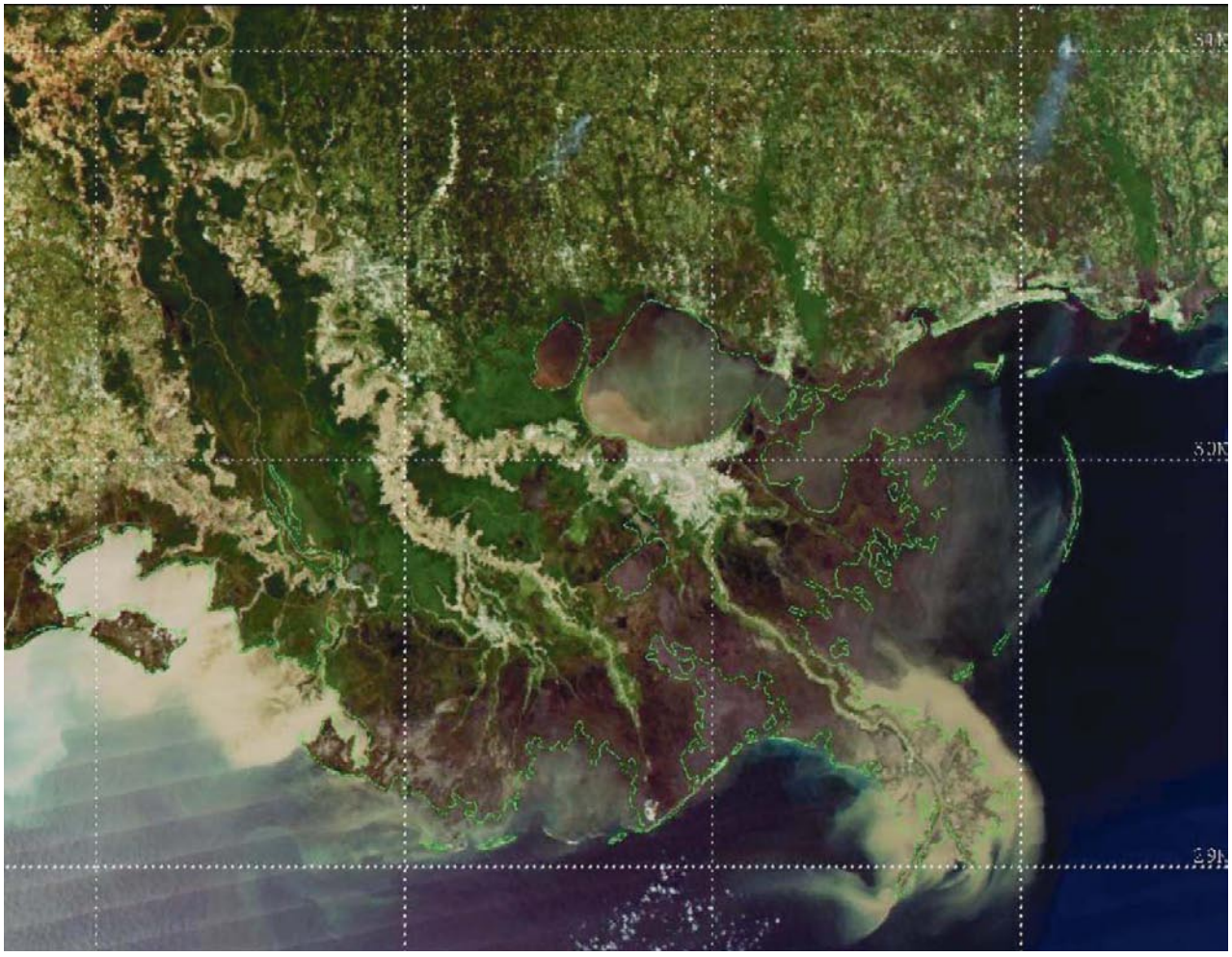

DOI: 10.1038/NGEO629

FIGURE 9

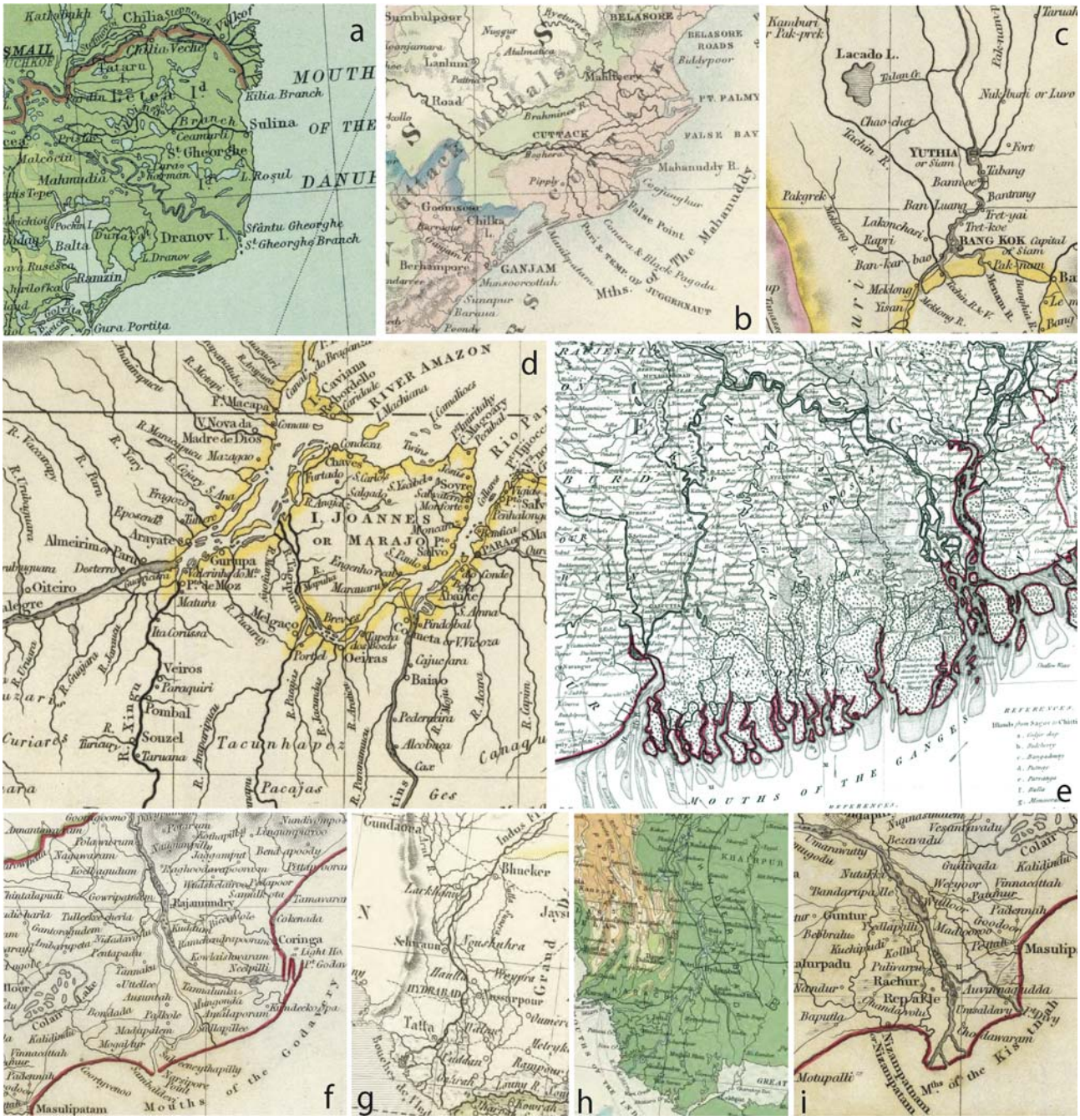

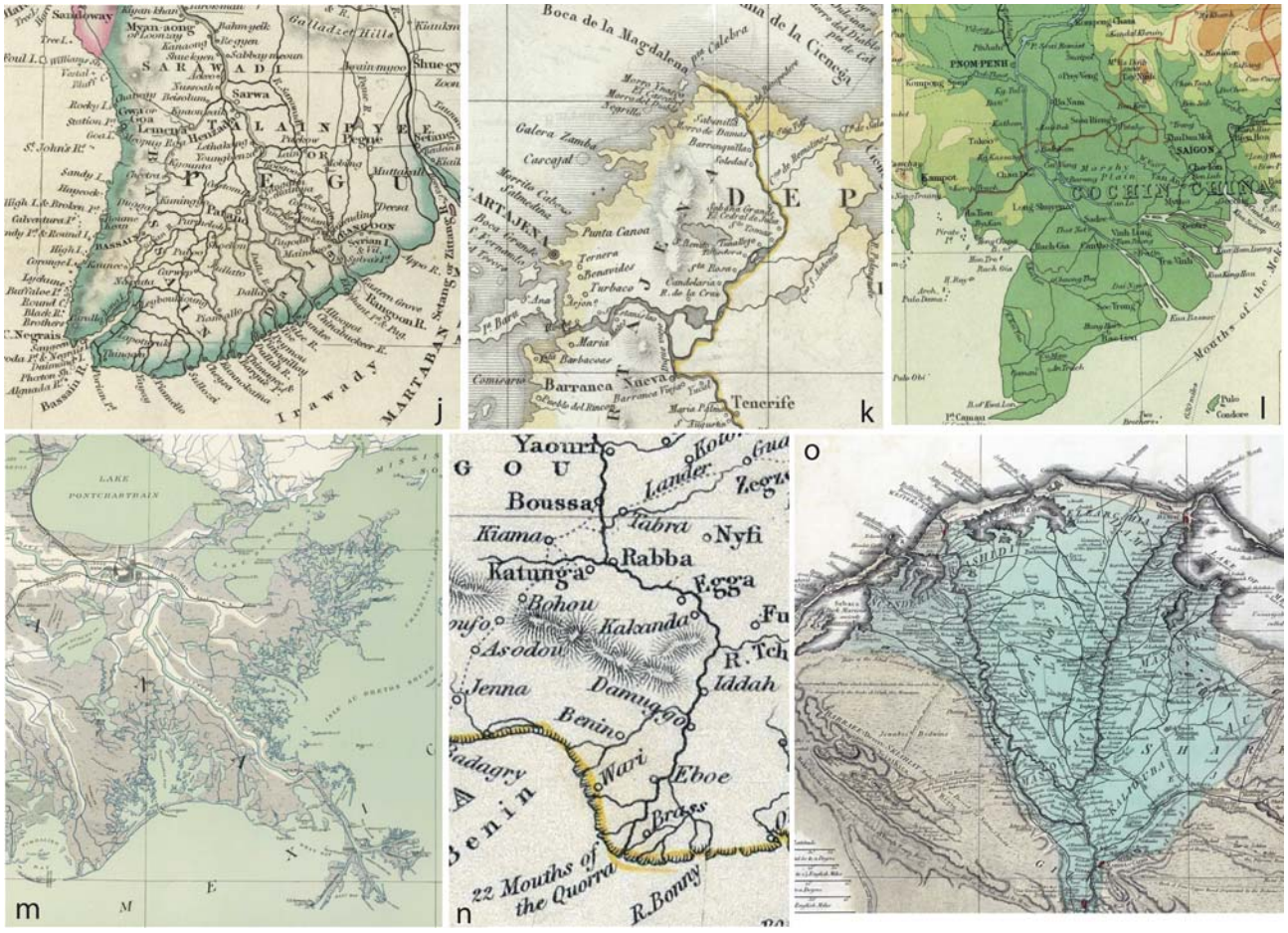
Myan-aong
SARAWADI
Sarwa
TALAINPYE
PEGU
Rangoon
Irawady
MARTABAN
j
Boca de la Magdalena
Galera Zamba
Carcajal
Punta Canoa
Ternera
Turbaco
Barranca Nueva
Tenerife
k
PNOM-PENH
SAIGON
COCHIN CHINA
Mouths of the Mekong
Pulo Condore
l
LAKE PONTCHARTRAIN
m
Yaourri
Boussa
Kiama
Tabra
Nyfi
Rabba
Katunga
Bohou
Kalzanda
Asodou
Jenna
Benino
Wari
Eboe
Brass
22 Mouths of the Quorra
R. Bonny
n
o

DOI: 10.1038/NGEO629

FIGURE 10



| | |
|---|---|
| **Sea Level Pressure** | Analysis 12 hour 24 hour 36 hour 48 hour |
| **500 mb Vorticity** | Analysis 12 hour 24 hour 36 hour 48 hour |
| **300 mb Height** | Analysis 12 hour 24 hour 36 hour 48 hour |
| **300-850mb Shear Magnitude** | Analysis 12 hour 24 hour 36 hour 48 hour |

## Tropical Advisory Archive

This is an archive of the TPC products, advisories and bulletins:

**Archive**

---

## Saffir-Simpson Scale

The chart color codes intensity (category based on Saffir-Simpson scale):

| Type | Category | Pressure (mb) | Winds (knots) | Winds (mph) | Surge (ft) | Line Color |
|---|---|---|---|---|---|---|
| **Depression** | TD | ----- | < 34 | < 39 | | Green |
| **Tropical Storm** | TS | ----- | 34-63 | 39-73 | | Yellow |
| **Hurricane** | 1 | > 980 | 64-82 | 74-95 | 4-5 | Red |
| **Hurricane** | 2 | 965-980 | 83-95 | 96-110 | 6-8 | Light Red |
| **Hurricane** | 3 | 945-965 | 96-113 | 111-130 | 9-12 | Magenta |
| **Hurricane** | 4 | 920-945 | 114-135 | 131-155 | 13-18 | Light Magenta |
| **Hurricane** | 5 | < 920 | >135 | >155 | >18 | White |

**NOTE:**Pressures are in millibars and winds are in knots where one knot is equal to 1.15 mph.



- For questions and information on this server, NOAAPORT and WXP, contact Dan Vietor at *devo@ks.unisys.com*
- For sales information on Unisys weather solutions, contact Robert Benedict at *robert.benedict@unisys.com*

*- Last modified February 1, 2007*

DOI: 10.1038/NGEO629